Graphene oxide nanocellulose composite as a highly efficient substrate-free room temperature gas sensor

Azlouk, Manel; Basyooni, Mohamed A.; Eker, Yasin Ramazan; Zor, Erhan; Bingol, Haluk

DOI
10.1016/j.rineng.2024.102228

Publication date
2024

Document Version
Final published version

Published in
Results in Engineering

Citation (APA)
Azlouk, M., Basyooni, M. A., Eker, Y. R., Zor, E., & Bingol, H. (2024). Graphene oxide nanocellulose composite as a highly efficient substrate-free room temperature gas sensor. *Results in Engineering*, *22*, Article 102228. https://doi.org/10.1016/j.rineng.2024.102228

Results in Engineering 22 (2024) 102228

Contents lists available at ScienceDirect

Results in Engineering

journal homepage: www.sciencedirect.com/journal/results-in-engineering

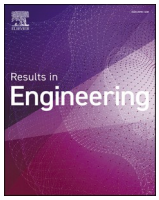

Graphene oxide nanocellulose composite as a highly efficient substrate-free room temperature gas sensor

Manel Azlouk [a,1], Mohamed A. Basyooni-M. Kabatas [b,c,d,*,1], Yasin Ramazan Eker [e,f], Erhan Zor [e,g], Haluk Bingol [e,f]

[a] Department of Chemistry, Graduate School of Natural Sciences, Necmettin Erbakan University, 42090, Konya, Turkey
[b] Department of Precision and Microsystems Engineering, Delft University of Technology, Mekelweg 2, 2628 CD Delft, Netherlands
[c] Department of Nanotechnology and Advanced Materials, Graduate School of Applied and Natural Science, Selçuk University, Konya 42030, Turkey
[d] Solar Research Laboratory, Solar and Space Research Department, National Research Institute of Astronomy and Geophysics, Cairo 11421, Egypt
[e] Science and Technology Research and Application Center (BITAM), Necmettin Erbakan University, 42140, Konya, Turkey
[f] Department of Basic Science, Faculty of Engineering, Necmettin Erbakan University, Konya, 42060, Turkey
[g] Department of Science Education, AK Education Faculty, Necmettin Erbakan University, 42090, Konya, Turkey

ARTICLE INFO

Keywords:
Bacterial nanocellulose
Graphene oxide
Reduced graphene oxide
Flexible room temperature gas sensor

ABSTRACT

This study introduces the development of novel, flexible gas sensors operating at room temperature (RT), utilizing a graphene oxide (GO) via the modified Hummers' method and bacterial nanocellulose (BNC) composite to enhance gas detection in industrial and environmental settings. The composite materials, denoted as GO@BNC, were synthesized with varying GO concentrations ranging from 2 % to 30 %, aiming to investigate their responsiveness to gases such as carbon dioxide (CO_2), oxygen (O_2), acetone (Ac), and ethanol (Eth). The prepared nanomaterials were characterized using FT-IR, Raman, TGA, SEM, and AFM techniques. The bandgap of Go ranges from 4.19, 3.47, 3.16, 2.79, and 2.48 eV for 2, 5, 10, 20, and 30 % GO concentrations, respectively. Notably, the sensor containing wt % of 20 % GO concentration exhibited remarkable sensitivity to Ac, achieving a 270 % increase in resistance at a concentration of 250 μL/L. Conversely, the sensor with a wt % of 30 % GO composition showed superior sensitivity to Eth, with a 420 % signal enhancement under similar conditions. Further modification of GO@BNC through mild reduction resulted in the formation of reduced graphene oxide (rGO@BNC) composites intended to assess the functional groups' impact on sensing performance. Our findings underscore the potential of GO@BNC composites as sustainable and efficient materials for fabricating eco-friendly flexible gas sensors and devices for detecting organic compounds.

1. Introduction

The instantaneous control of gas present in a workshop or merely in the atmosphere is requested to evaluate the possible risks that can be avoided with appropriate solutions. Gas sensors have been developed to get the actual gas concentration as soon as possible with the lowest cost and the most straightforward and adaptive working conditions. During the last decades, different gas sensors have been developed, among which those based on metal oxide are the most efficient [1,2]. Nevertheless, they are non-selective, rigid, and sometimes heated to more than 300 °C to give an exciting output signal [3]. Previous works have demonstrated that the electronic state [4] of the sensor, as well as its surface morphology [5], cracks [6] and chemical functionalities [7] have a significant impact [8]. Depending on the surface state, the gas adsorption influences the calibrated sensor's electrical properties, indicating the gas concentration around the sensor environment. Moreover, gas properties like size [9] and polarity [10,11] significantly affect its affinity to the sensor surface, making the sensor selectivity more complex; finally, due to the development of portative technologies, selective and flexible sensors that can work at RT where the scope of many research works [12,13].

One of the most ancient human inventions, paper offers an ideal flexible support for transmitting written text [14]. Nowadays, it has been involved within sensing or biosensing fields to predict diabetes or

* Corresponding author.
E-mail addresses: m.kabatas@tudelft.nl, m.a.basyooni@gmail.com (M.A. Basyooni-M. Kabatas).
[1] The second and first authors contributed equally.

https://doi.org/10.1016/j.rineng.2024.102228
Received 27 February 2024; Received in revised form 18 April 2024; Accepted 3 May 2024
Available online 9 May 2024

pregnancies via disposable test kits [15]. The main component of the paper is cellulose, a natural linear homopolymer based on β-D-glucopyranose monomers connected by β(1–4) glycosidic bonds. Cellulose chains are linked via van der Waals forces and hydrogen bonds involving a three-dimensional (3D) network of entangled fibrils [16]. The structure is called nano cellulosic when the fibrils' diameter is below 100 nm [17]. This biocompatible and biodegradable structure is transparent, lightweight, porous, hydrophilic, strong, and flexible [18–22]. Recent studies showed nanocellulose can be purely and naturally synthesized via specific bacteria such as Acetobacterxylinum in fruits or fruit products [23,24]. These bacteria deliver the purest form of cellulose fibers, characterized by the absence of other plant compounds like hemicellulose or lignin [24]. This natural way offers an excellent opportunity for eco-friendly bacterial nanocellulose (BNC) support.

In addition to its high surface-to-volume ratios, nanocellulose contains an essential number of functional groups [25], increasing its application potential [26–29]. In the first instance, nanocellulose has been used as filler in polymer matrixes for windmill blades, lightweight armor, or flexible batteries [30–32]. Then several investigations have been done for the development of electronic and optoelectronic devices such as transistors [33], surface-enhanced Raman spectroscopy [34], electrochromic devices [35], memory [36], capacitors [37], resistors [38], diodes [39], fluorescent paper [40], plasmonic metal nanoparticles for optical sensing [24], antennas [41], lithium-ion batteries [42], or Fe_3O_4 and $CoFe_2O_4$ magnetic nanopaper [43,44]. Concerning gas sensing, the low conductivity of nanocellulose is the main drawback [45,46]. To overcome these limitations, the contribution of several nanomaterials like silver (Ag) [47], gold (Au) [48], palladium (Pd) [49], iron oxide (FeO) [50], Platinum (Pt) [51] and various quantum dots [52] have been embedded in BNC composites. GO has recently received high attention in sensing applications [26,53–71]. For instance, CeO_2-GO composite has recently been used in humidity sensing applications [72], β-$Co(OH)_2$–Co_3O_4/GO for electrochemical sensing and energy storage applications [73,74], platinum nanoparticle-decorated reduced GO nanosheets in catalytic applications [75], while different properties enhanced in nickel/GO for electrocatalysts [76,77], magnetic GO nanocomposites in water applications [78], Pt-coated GO wrapped TiO_2 nanotube in the photoreduction of CO_2 [80] and air purification [79].

Due to the functional groups and the multiple bonds (π-electrons) within their structure, carbon-based nanomaterials are promising as fillers for BNC-based composites [80–83]. Conjugated multiple bonds and aromatic rings are responsible for the conductivity of carbon materials, which is needed to provide an electrical signal during the measurements [84,85]. Conversely, aromatic rings and functional groups play a double role for the composite-based gas sensors. Firstly, they can contribute to the mechanical properties of the composite, either by hydrogen bonds via oxygenated functions or π-π bonds between aromatic rings of fillers and BNC matrix [86]. Secondly, they can interact with the targeted gases via electronic densities and local polar distributions [87,88]. In the case of interaction between gas and composite, the electronic properties of composite will evolve, inducing a new electrical response. The BNC-based carbon-nanomaterial composites are all the more attractive because their preparation is relatively simple via a one-pot reaction with high quantum yields [89] using cheap, eco-friendly, and biologically compatible precursor compounds [90,91].

A recent study discusses using graphene nanomesh (GNM) functionalized with single-stranded DNA to detect chemical vapors, such as carboxylic acids, aldehydes, organophosphates, and explosives. The GNM field effect transistors (FETs) showcased improved vapor detection capabilities compared to standard graphene FETs due to oxidized edges and lattice defects. These DNA-decorated GNMs can discriminate between similar species with detection limits in the parts per million range, offering potential as sensors in electronic nose systems. For more details, you can view the article here [92]. Another study describes the development of a nanodevice using a single flake of nanoporous graphene to create a negative differential resistance (NDR) behavior [93]. This was achieved through a temperature-induced degenerate p-type GNP/rGO heterojunction. Key to this technology is the use of cellulose-based perforated graphene foams (PGFs), which demonstrate a band gap energy of about 1.8 eV. These PGFs are promising for future two-dimensional electronic nanodevices due to their stable and reversible NDR features at high temperatures. The device demonstrates potential in applications involving memory storage and THz frequency oscillation.

Based on this literature overview, developing green, low-cost, and flexible substrates for gas sensors is an opportunity to detect gases like acetone, ethanol, CO_2, or O_2, which are continuously present in our lifetime. This study demonstrated an *in-situ* electrical connected, biodegradable, and flexible gas sensor platform for RT measurements in the air using GO on CO_2, O_2, acetone, and ethanol environments. Different concentrations of GO were tested at a constant concentration of BNC, and the effect of the reduction of GO functional groups changed the composite surface affinity. Our innovative approach to the high surface-to-volume ratio of GO @ BNC may open a new way for next-generation gas sensor device applications.

2. Experimental section

2.1. Reagents and materials

Graphite powder (<45 μm, 99.99 %), H_2SO_4, H_3PO_4, H_2O_2, yeast extract, citric acid, peptone, and $KMnO_4$ were purchased from Sigma-Aldrich. Glucose, NaOH, and $MgSO_4.7H_2O$ were purchased from Merck. KH_2PO_4 was purchased from PS Park Ltd. $(NH_4)_2SO_4$ was purchased from Thomas Tyres Co. All reagents were purchased at the highest commercial purity and used without further purification. Besides, the solvents and the gases (acetone, ethanol, carbon dioxide, oxygen, and nitrogen) were provided in analytical purity degrees from different companies (Aldrich, Merck, Fluka, TCI, Alfa Easer, etc.). Distilled water with a resistance of 18.2 MΩ cm was obtained with the Direct-Q3 (Millipore) device. PTFE membranes (Millipore) with a pore of 0.22 μm were used in the filtration process. The GO was sonicated with a Bandelin ultrasonic bath. A Hettich centrifuge was used for the separation processes. For the structural characterization of the nanomaterials, the FT-IR spectrum was recorded on a Thermo Nicolet iS-20 spectrometer (USA). The Raman analysis was performed on a Renishaw-inVia Raman spectrometer (UK). Thermal measurements were obtained using Setaram Labsys Evo (France). Park System XE7 (South Korea) was used for the AFM and Zeiss Gemini SEM 500 for the SEM morphological characterization.

2.2. Preparation of the nanomaterials

2.2.1. Preparation of GO

GO was prepared from graphite powder following the modified Hummers' method [94]. For this procedure, 1 g of graphite was first added to a mixture of sulfuric acid and phosphoric acid (9:1). With gentle stirring and temperature maintained under 10 °C, 18 g of potassium permanganate was slowly added. After the mixture was entirely homogenous, the temperature was raised and retained at 50 °C for 8 h with continuous stirring. At the end of the 8 h, ice was added to the mixture to stop the reaction, and hydrogen peroxide was added to neutralize unreacted potassium permanganate until a change in the color of the suspension from dark brown to peach was observed. The obtained GO sludge was rinsed multiple times with distilled water until detecting sulfate ions by $BaCl_2$ was no longer possible. The product was further purified by repeating the rinsing procedure 15 times. Finally, GO was retrieved by centrifugation before being dried at 40 °C for a week.

2.2.2. Preparation of bacterial NanoCellulose (BNC)

Acetobacter Xylinum bacteria prepared BNC paper a customized culture medium: 50 g glucose, 5 g yeast extract, 5 g $(NH_4)_2SO_4$, 4 g

KH_2PO_4, and 0.1 g $MgSO_4.7H_2O$ were mixed in 1 L of distilled water, and the mixture was left for two weeks at 28 °C [24]. Then, the produced yellowish wet mat containing cellulose nanofibers, bacteria, and other impurities was treated with 5 wt% NaOH for 24 h at RT, followed by 1 wt% NaOH/0.2 wt% H_2O_2 for 1 h at 80 °C. Afterward, the resultant wet mat of pure bacterial cellulose nanofibers was rinsed with distilled water to remove the remaining chemicals and to obtain a transparent nanopaper (Scheme 1a).

2.2.3. Preparation of graphene-based bacterial cellulose composites (GO@BNC and rGO@BNC)

216 mg BNC was mechanically dispersed in 50 ml of distilled water until a homogeneous mixture was obtained. GO suspension was added to the bacterial cellulose depending on the desired GO concentration within the composite (from wt% of 2–30 %). After homogenization, the obtained mixture was filtered under a vacuum. The brown dense mixture was left to dry at 40 °C for a day on the membrane and then spontaneously separated, obtaining the GO@BNC composite (Scheme 1b). The flexible dried GO@BNC was stored under a vacuum to evaluate its gas sensing performances. After drying, the reduced graphene-based composite (rGO@BNC) was prepared by reducing the GO layers already presented in the GO@BNC composite. GO@BNC was soaked in a 5 % ascorbic acid solution for 48 h [95,96]. Afterward, the resultant materials (GO, BNC, GO@BNC, and rGO@BNC) were stored in the dark for characterization and further use.

2.2.4. Gas sensing setup

The sample integrated into the circuit was placed in a sealed chamber, and the electrical properties were measured using the gas inlet. The sample coated with silver paste was passed through a polymer-based cork cover and was connected to the wires, completing the circuit with a crocodile clip. There were connections on the cork where the heat probe, gas inlet, and outlet were integrated. This assembly was connected to the flask, which had a volume of 1 L, and then sealed, as shown in Fig. S1(a). During the measurement, acetone, ethanol, oxygen, and carbon dioxide gases were injected into the measurement chamber with a micro syringe and monitored by a gas flow meter.

The sensor was calibrated with nitrogen gas; then, it was included in the system with the tested gases to stabilize the sensor resistance. The output signal of the sensor (Potential/Resistance/Current) was monitored by the Keithley 2450 Source Meter instrument (20 mV and 10 nA sensitive) and the KickStart Keithley software, Fig. S1(b). The two-point probe station followed the development of the electrical properties of the circuit, so the information about inter-particle and particle-electrode conductivity was obtained utilizing current-potential curves.

3. Results and discussion

3.1. Characterization of nanomaterials

To confirm the graphene-based composite materials, firstly, the structural and morphological characterizations of the freshly synthesized GO were performed using FT-IR, Raman, TGA, SEM, and AFM techniques in detail **(**Supporting **information Figs. S2 and S3).** The results were found to be aligned with the literature [97]. As for the Raman spectrum of GO shown in the additional information section (Fig. S2 (b)), the characteristic peaks of carbon at 1349 and 1596 cm^{-1} were obtained. The ratio of intensities (I_D/I_G ratio) of these peaks (D and G peaks, respectively) attributed to Csp^3 and Csp^2 within the structure was determined to be 0.89.

The morphology of BNC has been characterized with SEM observations at different magnifications (Fig. 1a and b). As can be seen from the SEM images obtained at various magnifications, nanofibers without a specific woven mesh (randomly arranged) with radii in the range of 40–50 nm were observed as described in the literature for cellulose nanofibers obtained from bacteria [98,99]. The images in Fig. 1c and **d** are related to the morphology of GO@BNC, in which the GO layers were placed randomly within the cellulose fiber network. The intense interaction between the GO layer and BNC nanofibers (~60 nm) is visible at high magnification. It has also been emphasized in the relevant literature that this is due to the adhesion forces arising from hydrogen bonds between the oxygen-containing groups on the GO surface and BNC [100]. Similarly to GO@BNC, it was seen that the rGO layers also kept their positions in the cellulose fiber network (Fig. 3e and **f**). Although the interaction between the layer and the fibers is less significant, the distribution in the composite structure is still preserved due to

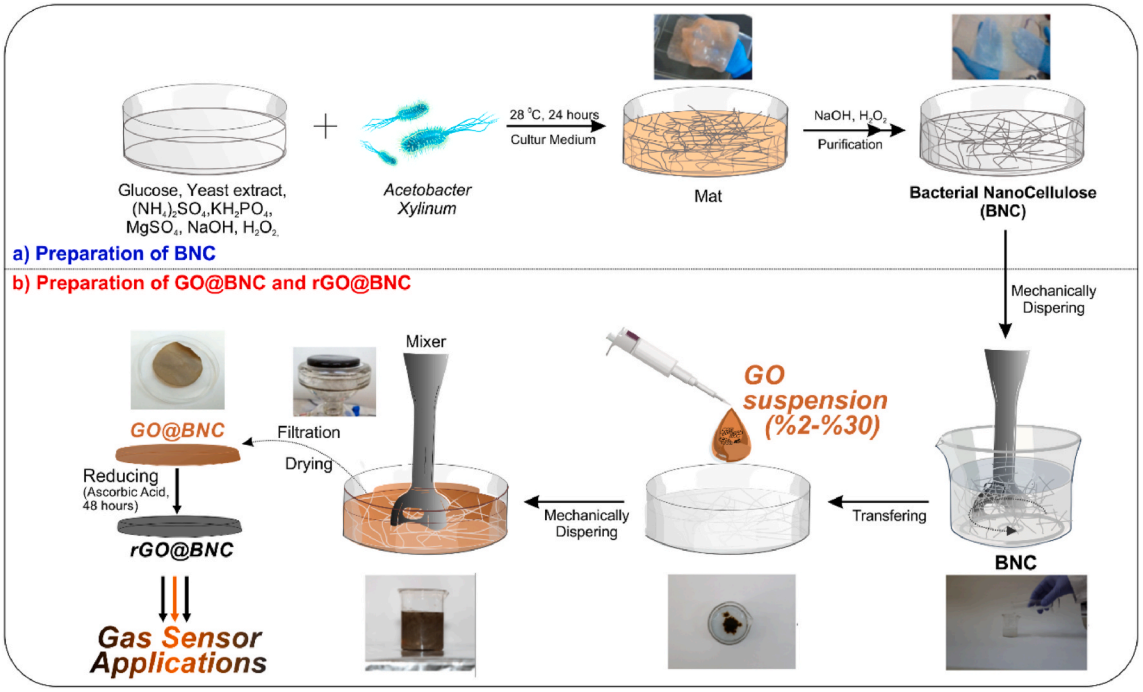

Scheme 1. Schematic presentation of the preparation of a) BNC and b) GO@BNC and rGO@BNC

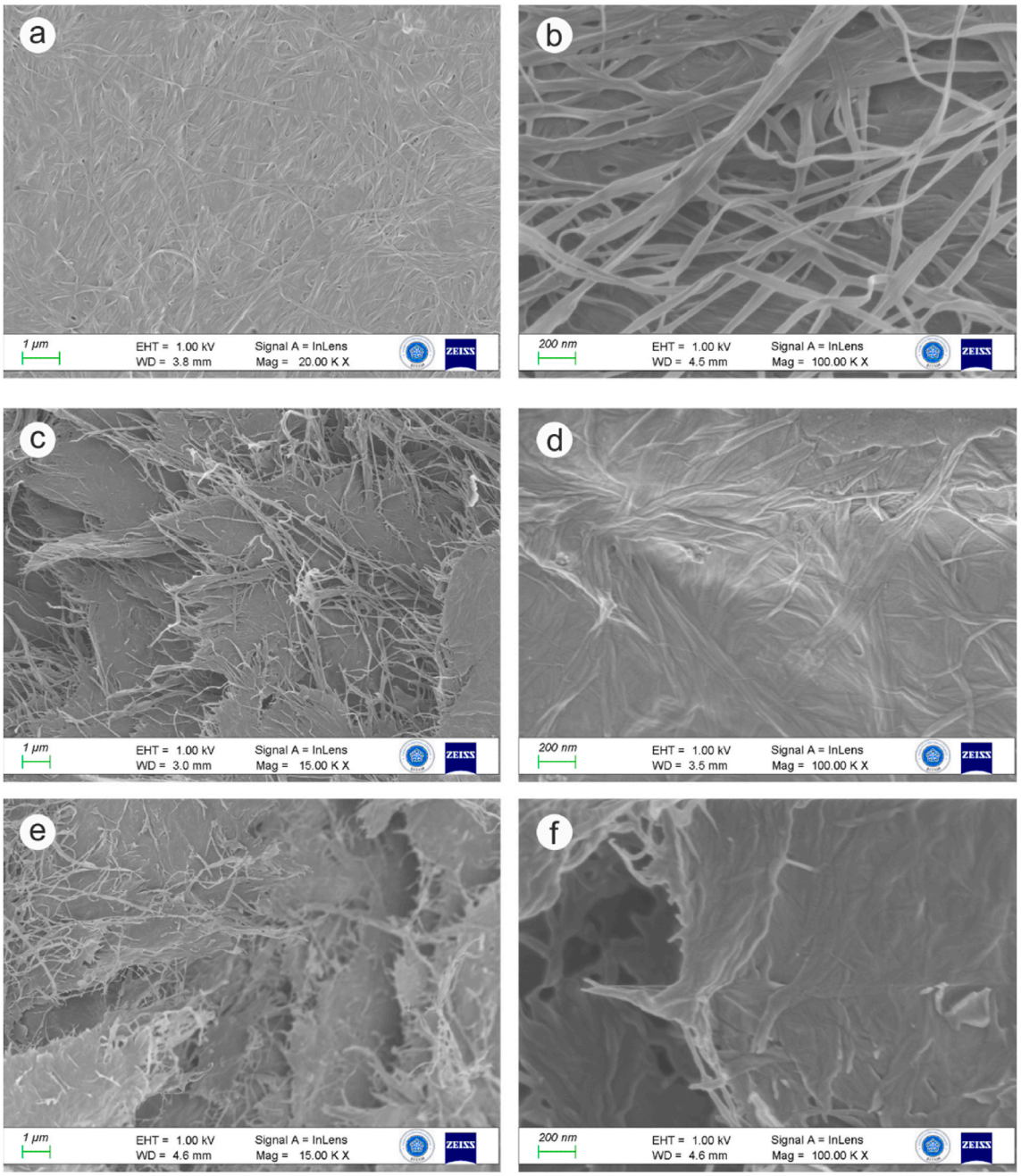

Fig. 1. SEM images of BNC (a,b), GO@BNC (c,d), and GO@BNC (e,f) at the different magnifications.

the dense entangled structure of the BNC nanofibers covering and wrapping the graphene-based layers [86].

The obtained FT-IR spectra between 4400 cm and 1 and 800 cm^{-1} are given in (Fig. S4) for the structural characterizations of BNC and the composite materials. For BNC, the characteristic strong and broad peak of O–H bonds in cellulose structure (hydroxyl groups) was observed around 3344 $cm^{-1,}$ while peaks around 2904 cm^{-1} show the stress vibrations of aromatic C–H bonds [101,102]. Temperature-mass change of TGA analysis obtained between 25 °C and 800 °C for structural characterization of BNC and the composite materials are also given in (Fig. S5). The BNC structure showed negligible dehydration-induced mass loss with the removal of adsorbed water in the 25–100 °C range, but its characteristic pyrolytic degradation is marked up to 378 °C [17].

3.2. Optical and electrical characterization

3.2.1. Optical and bandgap calculations

The optical absorption of the GO@BNC composites through the optical range of 200–1000 nm at RT has been measured using quartz cells. All samples were well-sonicated before the measurements to ensure good homogeneity. An absorption peak is observed at about 230 nm for the low GO concentrations reported in the literature [103]. A shift to a higher wavelength with increasing GO content was noted, as shown in Fig. 2a. The absorption peak enlargement observed at high GO concentrations is attributed to π- π* transition through the aromatic carbon-carbon bond and n- π* transition of the carbon-oxygen bond [104,105]. The absorbance-related bandgap (E_g) was calculated through the linear part of the $(\alpha h\nu)^2$ vs. $h\nu$ at $\alpha = 0$ (Fig. 2b). The bandgap ranges from 4.19, 3.47, 3.16, 2.79, and 2.48 ev for 2, 5, 10, 20, and 30 % GO concentrations, respectively. A bandgap of 2.78 eV has been reported in

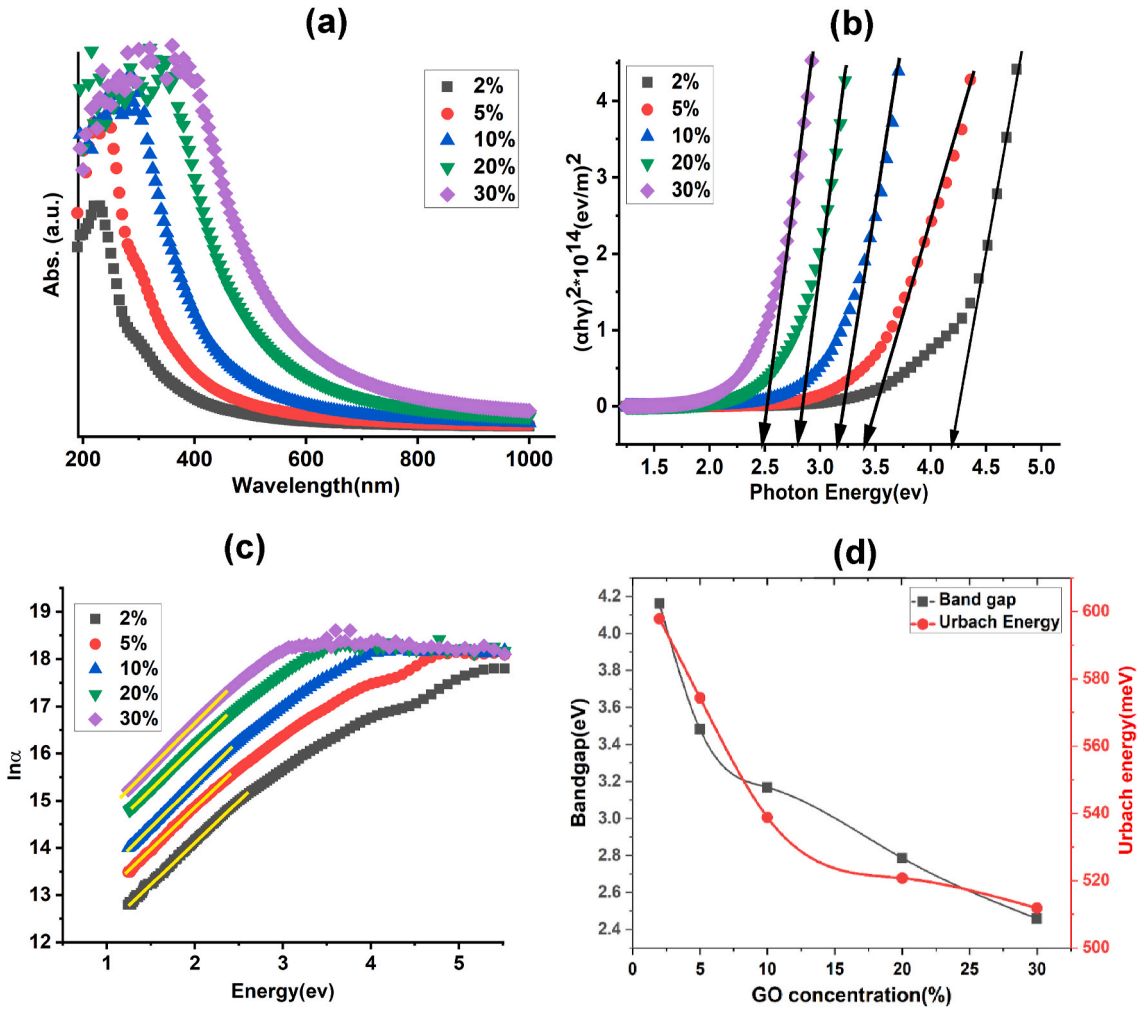

Fig. 2. Optical absorption of GO@BNC composites measured between 200 and 1000 nm, and the calculated curve obtained from the experimental results (a) $(\alpha h\gamma)^2$ vs. photon energy curves (b), ln α vs. energy (c) and change of the bandgap and Urbach energy by GO content in the GO@BNC composites (d).

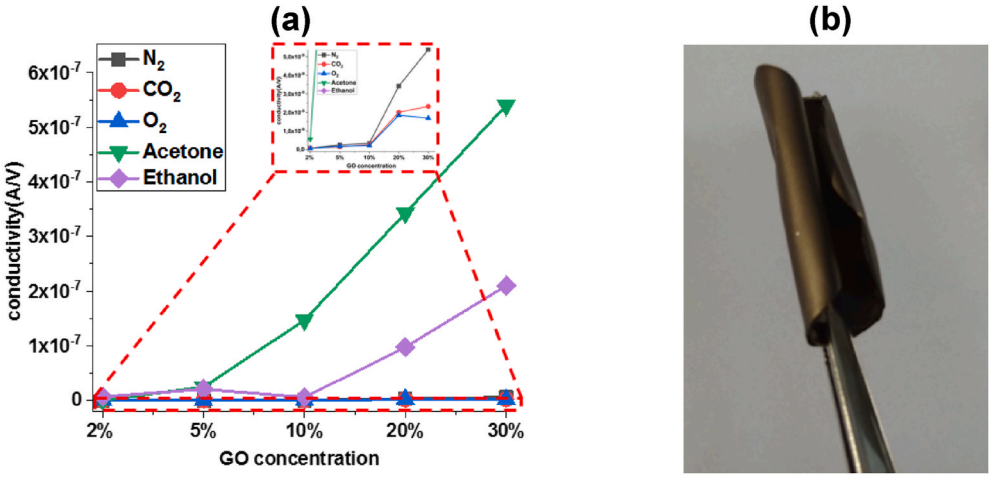

Fig. 3. Evolution of the conductivity values at 5V bias of GO@BNC composites a with different GO concentrations (a) The photo of bending capability of 20 % GO@BNC composite (b).

the literature for thin films containing about 30 % GO [106]. With increasing the GO content, a shrink in the bandgap values was observed due to the expected high electron mobility and concentrations at high GO content. This evolution in the bandgap value is essential in the gas sensing kinetic measurements.

The band tail width in the valence and conduction band can be determined from the equation of Urbach energy; $E_u = \left[\frac{d(\ln(\alpha))}{d(h\nu)}\right]^{-1}$ and

can be calculated from the linear fitting of ln(α) vs. energy and taking the slope (Fig. 2c). E_u is used to estimate the material's disorder, the higher disorder involves a lower E_u [107,108]. Structural disorders, stoichiometry imperfections, and surface passivation are defects associated with Urbach's energy [109–112]. Thus, the change of the band gap (4.19–2.48 eV) and Urbach energy (598–512 meV) by the GO concentration (2–30 %) given in Fig. 2d can be attributed to the increase of the structural disorder with increasing the GO content in the composite. Due to their weak interaction, GO sheets probably tend to agglomerate with their concentration, increasing the structural disorder.

3.2.2. Current-voltage (I–V) measurements

Fig. S6 shows composites' forward current-voltage (I–V) characteristics with GO content of 2 %, 5 %, 10 %, 20 %, and 30 % under N_2, O_2, CO_2, acetone, and ethanol atmosphere at RT. Under the O_2, N_2, and CO_2 atmospheres, which are nonpolar molecules, the intensity reach for all samples is below 30 nA, even at a 5V bias voltage. It can reach μA scale (1.6 μA for 20 % GO@BNC under acetone) when composites are tested under acetone and ethanol, which are polar molecules. Fig. S6 (a) For the 2 % GO composite, the current response (measured in microamps, μA) to the applied voltage (V) shows significant sensitivity to ethanol and acetone, with negligible response to N_2, CO_2, and O_2. Fig. S6 (b) With 5 % GO, the sensitivity to acetone and ethanol remains, with a slight increase in current, indicating improved conductivity or interaction with these gases compared to 2 % GO N_2, CO_2, and O_2 responses are still minimal. Fig. S6 (c) At 10 % GO, the current response to acetone and ethanol is much larger, suggesting that the increased GO content improves the interaction with these gases even more. The responses to N_2, CO_2, and O_2 are somewhat more pronounced but still relatively low. Fig. S6 (d) The 20 % GO composite shows a further increase in current for acetone and ethanol, indicating a continued improvement in gas interaction. There is also a slight response to N_2, CO_2, and O_2, though these remain significantly lower than the response to acetone and ethanol. F ig. S6 (e) Finally, the 30 % GO composite shows a lower current response to all gases compared to the 20 % GO composite, possibly indicating a saturation effect where too much GO could be reducing the overall sensitivity of the composite or affecting the stability of the sensor. Overall, the patterns in the curves suggest that the GO@BNC composites have a selective response to acetone and ethanol, with the sensitivity generally increasing with the GO content up to a certain point (20 % GO seems optimal based on these curves) and shows stability with minor errors [113]. At 30 % GO, there may be too much material, which could be detrimental to the sensor performance, indicated by the lower current levels and less bending stability.

On the other hand, the conductivity values of all samples except the composite 2 % GO@BNC are higher under acetone than in an ethanol atmosphere. The conductivity increase is more marked under acetone with samples with more than 5 % GO content. In comparison, this behavior is observed for samples with a GO ratio above 10 % (Fig. 3a). This suggests that the composites' conductivity depends on the presence of graphene-based materials. These preliminary results demonstrate that GO@BNC composites are promising for the detection of both acetone and ethanol. Furthermore, the Ohmic contact response, in other words, the linear conductivity evolution, observed by increasing the bias voltage, is a good sign for the concentration detection of both gases. Finally, especially for composites loaded with 20 % and 30 % GO bending, it does not involve breaks, which is promising for preparing flexible sensors. The resulting membrane-like composite materials (Fig. 3b) have been used after being cut to the required dimensions.

3.2.3. Resistance-time measurements

The stability of the prepared nanomaterials was explored by studying the measurements of resistance-time behavior. As shown in Fig. 4a and b, the performance under acetone and ethanol atmosphere has been mainly evaluated, respectively. However, the electrical behavior under O_2, N_2, and CO_2 has also been considered due to their presence in the air (Fig. S7). It is worth noting that N_2 has been used as a purging gas after adsorption of the target gas. The characteristic resistance-time (R-t) curve was obtained at 5V bias voltage. GO@BNC composites with different concentrations of GO (except 2 % GO@BNC) have relatively stable and close resistance values with time towards all gases. The slight increase observed for the 2 % GO@BNC sample is probably due to the late and low diffusion, which delays the adsorption of gas molecules on the GO inside the composite. On the other hand, lower resistance and higher stability were observed for 20 % and 30 % of GO-containing composites, which is why the work has been focused on both samples below.

3.3. Gas sensing performances

3.3.1. Dynamic measurements of the GO-based composites

The evolution of the sensor resistance with time and the gas amount introduced inside the measurement system at RT determines the gas sensing performance. For each sensor and each target gas, the chamber first flowed with an N_2 purge gas; after that, a known gas amount (from 50 to 250 μL) was introduced to the chamber. For each volume, the resistance is followed for 60 s. After that, N_2 purging gas was re-introduced in the chamber for 60 s, and the next step started with a further amount of target gas. A relatively linear evolution from a minimum to maximum resistance value (or vice-versa) is needed to evaluate the sensor's sensibility. Moreover, the sensing time is considered finished when the resistance decreases or increases to reach a difference of 90 %.

The sensitivity of the sensor was calculated according to equation

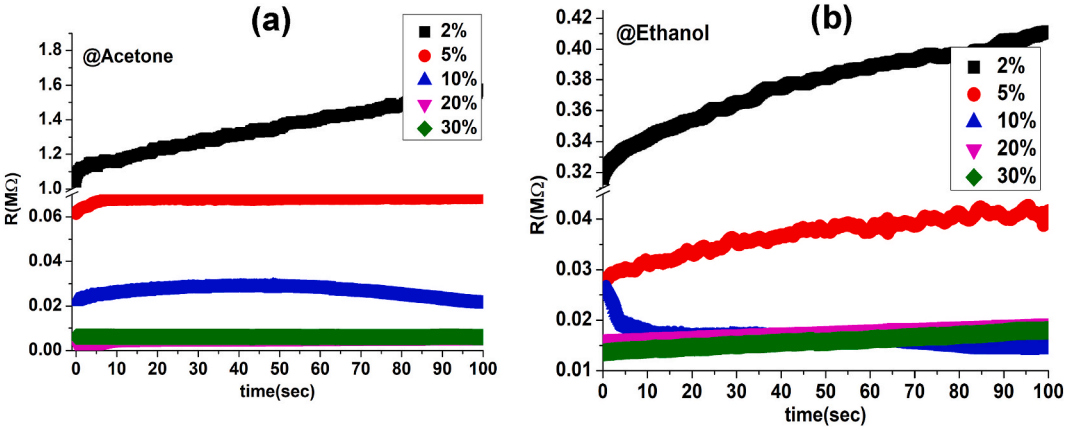

Fig. 4. Resistance-time (R-t) curve of GO@BNC with GO content of 2 %, 5 %, 10 %, 20 %, and 30 % towards acetone (a) and ethanol (b).

(1), which shows the ratio of the difference between the resistance measured with nitrogen (R_{N2}) and the resistance measured with the working gas ($R_{target\ gas}$) [105]:

$$S(\%) = \frac{R_{target\ gas} - R_{N_2}}{R_{N_2}} * 100 \quad (1)$$

The results of lower GO content and those obtained under O_2 and CO_2 are not prominent (non-linear evolution or too small resistance difference). Therefore, the measurements for the sensors with the lowest GO content under O_2 or CO_2, including samples with high GO content, have been presented. The dynamic sensor measurements of the composite containing 20 % and 30 % GO under acetone and ethanol are considered in detail. Since acetone and ethanol are reducing gases [108, 114], their adsorption involves an increase of free electrons on the samples, i.e., a decrease in the composite resistance.

For 20 % GO@BNC and under both gases, a comparable evolution

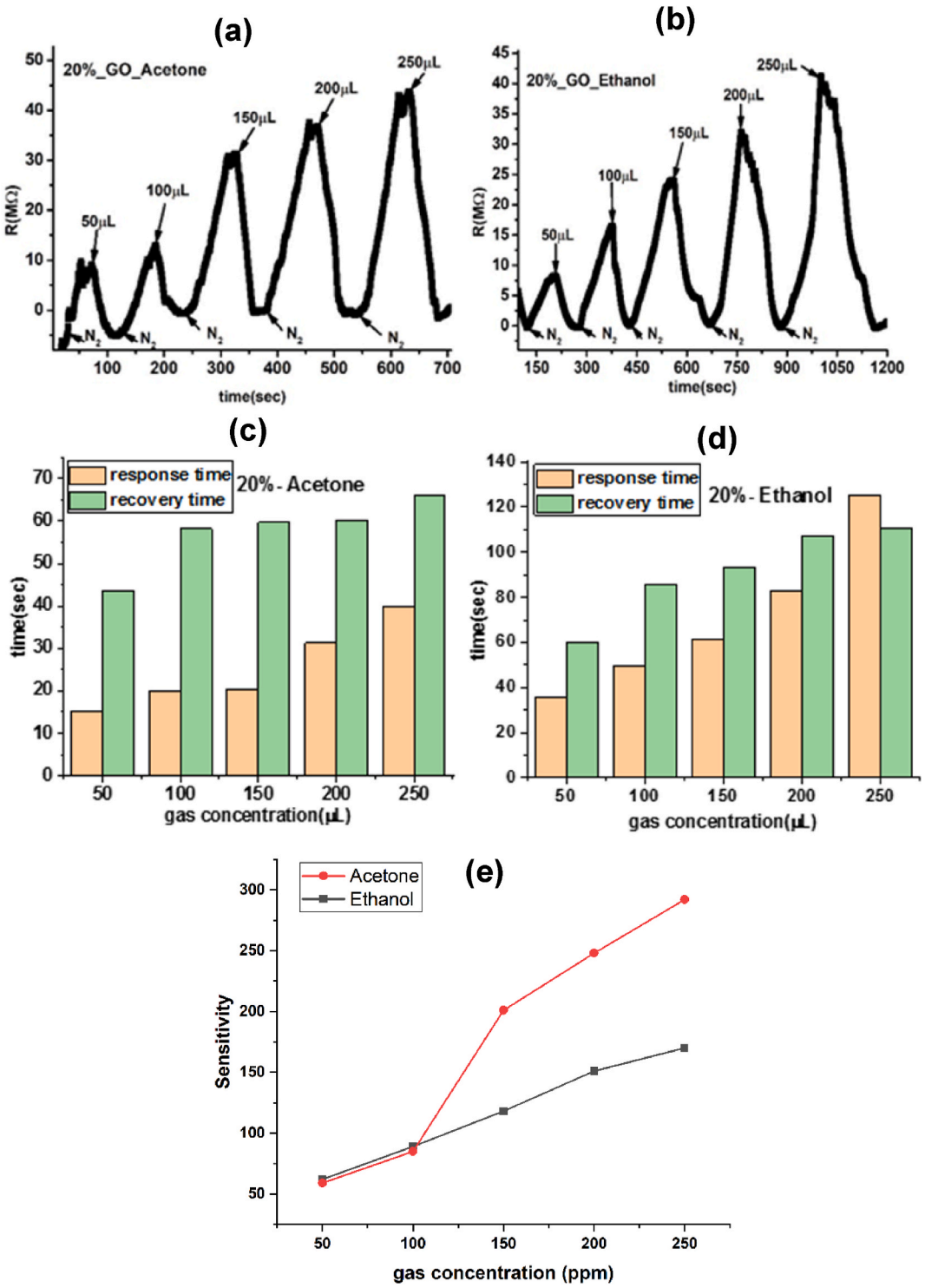

Fig. 5. Dynamic gas sensing investigation of 20%GO@BNC under acetone and ethanol atmosphere by increasing the gas concentration. Evolution of the composite resistance with (a) acetone and (b) ethanol. Evolution of the response/recovery time with (c) acetone and (d) ethanol. Evolution of the sensitivities (e) with both gases.

trend is observed between the highest and the lowest resistance values with the increase of target gas concentration (Fig. 5a and b)). After each gas injection within the chamber, the lower resistance is reached at approximately the same value. Therefore, it can be considered that gas molecules are completely adsorbed and desorbed on all the active sites offered by the composite. Furthermore, the adsorption or response time is faster than the desorption or recovery time; in other words, gas molecules interact relatively well with the active sites (Fig. 5c and d). The formers are probably on the GO surface since the electrical properties of the composite depend on the presence of GO, and they are modified with gas adsorption. Moreover, different active sites contribute to the adsorption of ethanol and acetone since the composite does not present the same sensibility evolution towards both gases, significantly above 100 ppm gas concentration (Fig. 5e). Sensitivity can reach almost 300 % for acetone while for ethanol is at 170 %. The adsorption between the GO and the gases is either electrostatic because of the polarity of both gases or via hydrogen bonding.

The hydrogen bonding is highly probable because of the active sites on GO, which are carbonyl (C═O) and hydroxyl (−OH) based. These functions can interact separately with the carbonyl group of acetone and the hydroxy group of ethanol via hydrogen bonds (C═O——H−O). The carbonyl and hydroxyl active sites present at the surface of GO seem to play a significant role in the gas sensing of ethanol and acetone, respectively. The gas sensing measurements were done with 20 % rGO@BNC, obtained from the composites' mild reduction to confirm these observations.

The stability of our gas sensors, particularly after numerous sensing cycles, represents a crucial aspect of our study. As highlighted in the supplementary information (Fig. S8), our experimental data comprehensively analyzes the resistance-time behavior under continuous exposure to various gases for 100 s at a bias voltage of 5V. This analysis includes the effects of O_2, N_2, CO_2, acetone, and ethanol gases commonly present in the air, with nitrogen used as a purging gas post-adsorption. Our findings indicate that the GO@BNC composites, except for the variant with 2 % GO, exhibit remarkable stability in resistance values over time across all tested gases. The minor resistance increase observed in the 2 % GO@BNC sample is likely attributed to the hindered diffusion and delayed adsorption of gas molecules within the composite. In contrast, composites containing higher concentrations of GO (20 % and 30 %) demonstrated lower resistance and enhanced stability. This superior performance led us to focus our investigations on these two compositions. This sustained sensor stability, especially after multiple cycles, underscores the potential of GO@BNC composites for reliable and consistent gas sensing applications. Our ongoing research aims to elucidate further the mechanisms underpinning this stability, paving the way for developing durable and efficient gas sensors.

3.3.2. Gas sensing performance of 20%rGO@BNC

Our study meticulously analyzed the interplay between the functional groups, electronic properties, and morphological features of GO embedded in bacterial nanocellulose (BNC) composites and their impact on gas sensing capabilities. A significant correlation was observed where oxygen-containing functional groups on GO, such as hydroxyl (-OH) and carboxyl (-COOH) groups, directly influenced the sensor's sensitivity and selectivity towards specific gases. For instance, the interaction mechanism of acetone and ethanol with the sensor surface could be attributed to these molecules' varying affinities towards different functional groups. Acetone showed a higher affinity towards –OH groups, while ethanol was more responsive to carbonyl (=O) groups.

Additionally, incorporating GO into BNC enhanced the electrical conductivity due to the narrowing of the band gap. It introduced a higher density of active sites for gas adsorption, thereby improving the composite's gas-sensing performance. Due to varying GO content, bandgap modulation was found to play a crucial role in the sensitivity towards gases, with a lower bandgap correlating to enhanced sensitivity. The structural characteristics of the GO@BNC composites, such as porosity and surface area, were also crucial in determining the gas sensing performance. A higher GO content increases area and porosity, which facilitates this. This is evident in the superior sensitivity of composites with higher GO content towards ethanol and acetone.

The TGA and FTIR results of BNC and 20 % GO-loaded composites before and after the reduction process demonstrate that the functional groups are primarily removed from GO, and some oxygenated groups are still present. Therefore, the electrical properties and, above all, the sensitivity towards ethanol and acetone of the composite 20%rGO@BNC have been completely changed after reduction. According to the I–V measurements under different gas atmospheres, the conductivity of the composite decreases dramatically since the current rates decrease from microampere (Fig. S7d) to nano ampere scale (Fig. 6a). Moreover, the Ohmic behavior of the composite under acetone is less pronounced. The current intensities are almost 10 times lower than those measured under ethanol. Furthermore, the composite resistance is very high and does not change proportionally with the gas injected within the chamber, contrary to the behavior under ethanol (Fig. 6b and c). Nevertheless, a well-defined dynamic behavior is obtained only after stabilizing the sensor for more than 800 s. Moreover, the evolution of resistance between the presence of nitrogen and ethanol is very low at about 0.1 MΩ inducing a low sensitivity below 3 % (Fig. 6d). Finally, the short response and recovery time demonstrate a fast adsorption/desorption process (Fig. 6e). The presence of less functional groups induces not only their quick saturation but also less polar interactions with ethanol which can slow down the gas diffusion.

3.4. Limit of detection and selectivity

The limit of detection (LOD) can be defined as the smallest concentration of an analyte that can be reliably distinguished from background levels $LOD = 3\frac{\sigma}{S}$, where 'σ' represents the standard deviation of the background signal in the absence of the analyte, and 'S' denotes the slope of the sensitivity curve, reflecting the sensor's response as a function of the analyte concentration. According to our calculations, the LOD for acetone has been determined to be 1.89 sccm, while it stands at 1.09 sccm for ethanol. Our detection limit values are comparable to the literature reviews of different gas-sensing gases.

The selectivity measurements of the sensors are addressed in terms of electrical IV curves and sensor response by considering four different gases: O_2, CO_2, acetone, and ethanol, as in Fig. S8. The response curves of O_2 and CO_2 show significantly lower and more erratic changes in resistance compared to those of acetone and ethanol. This indicates that the sensor's selectivity for acetone and ethanol is much higher than for O_2 and CO_2. Acetone and ethanol produce sharp, prominent peaks corresponding to their respective concentrations, demonstrating the sensor's higher sensitivity and selectivity towards these compounds. The consistent and proportionate increase in resistance with higher concentrations of acetone and ethanol suggests good selectivity, as the sensor responds more robustly and predictably to these substances. Looking at the response curves for acetone and ethanol, acetone does exhibit a higher response than ethanol at equivalent concentrations. The peaks in the response curve for acetone are higher and sharper, indicating a quicker response to changes in concentration. This higher and sharper response suggests a more excellent selectivity towards acetone. Selectivity measures a sensor's ability to respond to a specific analyte in the presence of other substances. In this case, the sensor seems more selective towards acetone over ethanol.

3.5. Sensing mechanism

Gas sensors are characterized by the evolution of their electrical properties in the presence of targeted molecules. The device sensitivity is related to the amount of gas molecules adsorbed onto the surface of active material. The van der Waals interactions or hydrogen bonding are

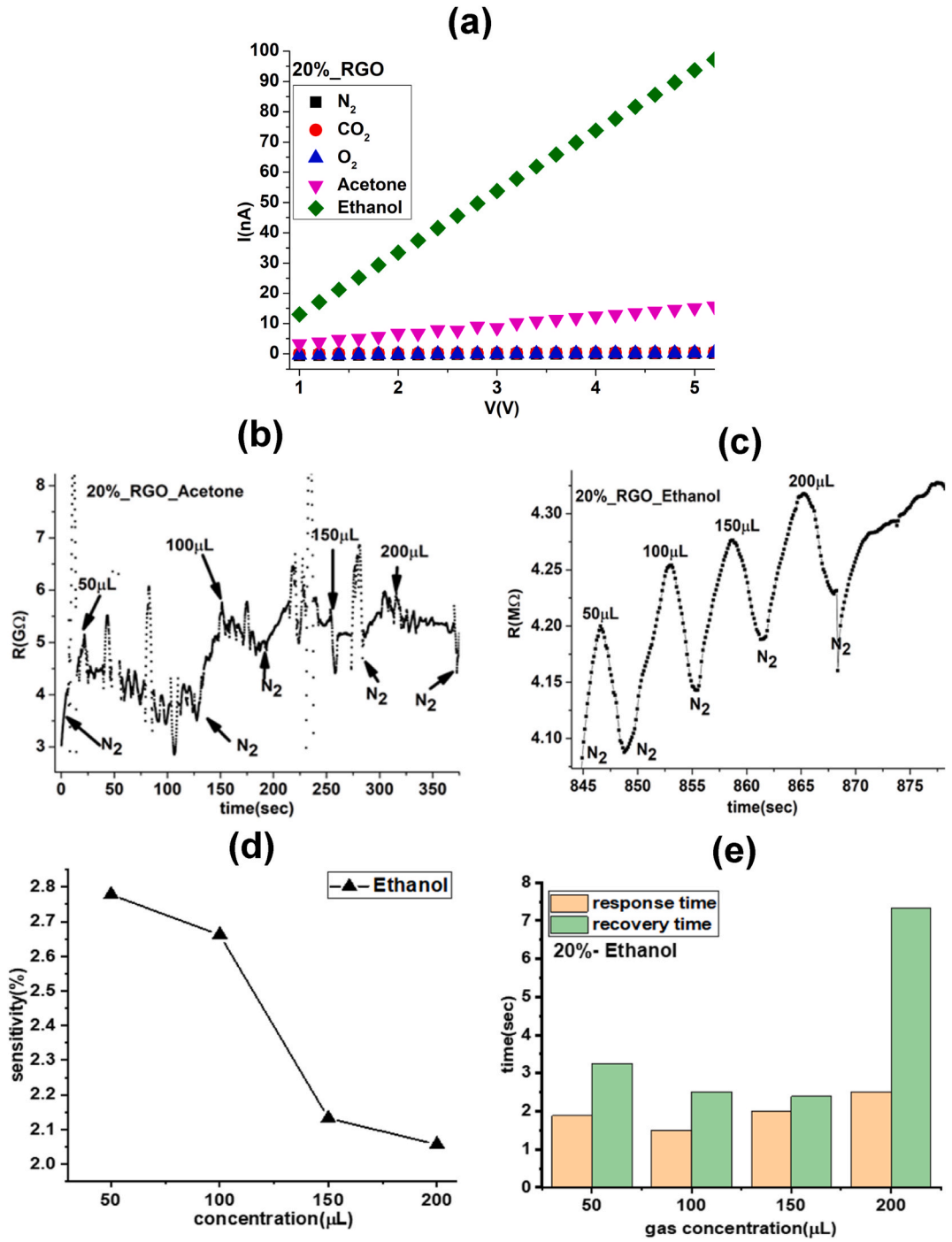

Fig. 6. I–V measurements (a), dynamic sensing behavior under acetone (b) and ethanol (c), sensitivity (d), and response/recovery time (e) under ethanol atmosphere of 20%rGO@BNC composite.

mainly involved during the molecule adsorptions, depending on the surface functional groups that modify the surface electronic density. Furthermore, the free space within the sensor's active material allows a faster diffusion of gas molecules, increasing the gas sensor's response time and sensitivity.

In this work, the gas sensor active material is a composite material prepared with a porous and flexible BNC containing mainly –OH and -C-*O*-C- functional groups and GO with –OH, C═O, -C-*O*-C- and –COOH functional groups. According to the literature, –OH and -C-*O*-C- functions are preferentially present within the graphene plane, while –COOH are on the edge groups. Due to the electronegativity difference between C ($\chi = 2.55$) and O ($\chi = 3.44$), both materials are polar, inducing an effective interaction between them during the composite formation. The gas sensor performance of the composites has been separately investigated with oxygen, carbon dioxide, ethanol, and acetone gases. The intrinsic properties of all these compounds are suitable for understanding the gas-sensing mechanism. First of all, the steric effects can be estimated due to their molecular volumes: O_2 (~23 Å^3), CO_2 (~38 Å^3), ethanol (~59 Å^3), and acetone (~73 Å^3). Secondly, the influence of the van der Waals interactions has been investigated since O_2 and CO_2 are nonpolar molecules, while ethanol (1.66 D) and acetone (2.69 D) are polar. Thirdly, hydrogen bonding has been evaluated since O_2, CO_2, and acetone contain O elements, and ethanol contains –OH groups at their extremity. The hydrogen bonding influence has been emphasized by

investigating the sensing performance with 20%rGO@BNC composite. As a result, the obtained results can be summarized as follows.

- The gas sensing responses are only meaningful with the polar molecules, which are also the biggest. The I–V curves under the O_2 and CO_2 atmosphere are similar to the ones under the N_2 atmosphere used during the sensor recovery. Moreover, O_2 and CO_2 are the smallest molecules, confirming that the steric effect does not influence the gas-sensing mechanism.
- By increasing the GO ratio from 2 wt% to 30 wt% within the composite, the detection of acetone is growing continuously. The BNC matrix prevents the agglomeration of GO, which is the source of the introduction of functional groups within the composite.
- Similarly to acetone, ethanol sensing is improved by increasing the GO ratio within the composite. Nevertheless, the evolution of sensing performance with the GO ratio is different. The sensitivity is weaker for the lowest GO ratio and abruptly increases with ratios greater than 20 %.
- Due to the difference in behavior during gas sensing of the two polar organic molecules, the influence of the Van der Waals interactions is weak. Furthermore, the most significant molecule, acetone, is better detected than ethanol. Thus, hydrogen bonding seems to be the most effective interaction.
- The hydrogen bonding with acetone is mainly triggered by –OH functions present at the GO surface, while for ethanol, C═O, -C-*O*-C- and –COOH groups are involved. As known in the presence of ethanol, the carboxylic groups turn into ester, favoring the interaction with further ethanol introduced within the chamber. Therefore, the interactions of acetone and ethanol molecules are in different positions of the GO materials.
- The mild reduction of GO-induced rGO on which the –OH groups are removed, and only the C═O group is present. That is why only ethanol is detected with 20%rGO@BNC composite and not acetone.
- The increase of the GO ratio within the composite not only percolates the composite whose resistivity is sharply decreasing but also introduces active sites that can detect ethanol and acetone. Furthermore, the flexibility of BNC decreases to form a rigid composite with 30 % GO. The BNC contains –OH functions, which induce hydrogen bonding with C═O, -C-*O*-C- and –COOH of GO. These interactions are responsible for the stability of the composite but also delay the availability of functional sites for ethanol detection. It is expected that direct hydrogen bonding between –C═O, -C-*O*-C- and covalent bonding when –COOH are involved.
- It is essential to mention that the gas molecules can interact with the functional groups via hydrogen bonding and be used as a hydrogen sensor. Those interactions have been implied in the literature with improved hydrogen sensing performance with the functional groups of graphene-based materials [115,116]. However, this study demonstrates that both functional groups present at the surface of graphene-based materials and the oxygen present within the gas molecule structure are involved in forming hydrogen bonds between gas molecules and sensing materials.

4. Conclusion

The efficacy of gas sensors hinges on their electrical conductivity and the presence of active sites for molecular interaction. Our study harnesses bacterial nanocellulose (BNC) for its flexible and fibrous structure, enhancing the electrical properties and surface area available for gas interaction. At the same time, GO is a functional additive, introducing reactive sites on the sensor's surface. The optimal inclusion of at least 20 % GO has been identified to achieve significant sensitivity levels—approximately 170 % for ethanol and 290 % for acetone at a concentration of 250 ppm. The mechanism underlying these interactions is primarily through hydrogen bonding; acetone is drawn to –OH groups, whereas ethanol prefers areas devoid of hydrogen, such as = O or –COC– groups. This selective sensitivity was further substantiated by tests involving rGO@BNC composites, which possess predominantly hydrogen-free functional groups, demonstrating exclusive sensitivity to ethanol. Our GO@BNC-based sensors demonstrate considerable potential for high-precision detection of acetone and ethanol, which is critical for maintaining safe conditions in research and development settings by enabling timely ventilation when concentrations approach hazardous levels. Moving forward, we aim to explore the sensors' capability to differentiate and quantify ethanol and methanol distinctly. Such advancements could revolutionize the rapid and straightforward identification of adulterated alcohols, offering significant safety and quality control benefits in various applications.

CRediT authorship contribution statement

Manel Azlouk: Writing – original draft, Validation, Methodology, Formal analysis, Data curation. **Mohamed A. Basyooni-M. Kabatas:** Writing – review & editing, Writing – original draft, Visualization, Validation, Methodology, Investigation, Formal analysis, Data curation, Conceptualization. **Yasin Ramazan Eker:** Writing – review & editing, Visualization, Validation, Supervision. **Erhan Zor:** Writing – review & editing, Visualization, Validation, Supervision, Project administration, Investigation, Conceptualization. **Haluk Bingol:** Writing – review & editing, Visualization, Validation, Supervision, Project administration, Methodology, Investigation.

Declaration of competing interest

The authors declare that they have no known competing financial interests or personal relationships that could have appeared to influence the work reported in this paper.

Data availability

Data will be made available on request.

Acknowledgments

This study was supported by The Scientific and Technological Research Council of Turkey (TÜBİTAK), Grant No: 119M043.

Appendix A. Supplementary data

Supplementary data to this article can be found online at https://doi.org/10.1016/j.rineng.2024.102228.

References

[1] S.M. Majhi, A. Mirzaei, S. Navale, H.W. Kim, S.S. Kim, Boosting the sensing properties of resistive-based gas sensors by irradiation techniques: a review, Nanoscale 13 (2021) 4728–4757, https://doi.org/10.1039/D0NR08448D.
[2] J. Park, H. Lim, J. Yea, C. Ryu, S. Jung, R.J.-R. in, undefined 2024, Kirigami-inspired gas sensors for strain-insensitive operation, Elsevier, in: J. Park, H. Lim, J. Yea, C. Ryu, S.I. Jung, R. Jana, K.I. Jang, H. Keum, H.J. Kim (Eds.), Results in Engineering, Elsevier, 2024 (n.d.), https://www.sciencedirect.com/science/article/pii/S2590123024000586. (Accessed 14 April 2024).
[3] Y. Liu, J. Parisi, X. Sun, Y. Lei, Solid-state gas sensors for high temperature applications – a review, J Mater Chem A Mater 2 (2014) 9919–9943, https://doi.org/10.1039/C3TA15008A.
[4] M. Liu, Adsorption behavior of Ni-doped ZnO Monolayer upon SF6Decomposed components and effect of the applied electric field, ACS Omega 5 (2020) 24118–24124, https://doi.org/10.1021/ACSOMEGA.0C03663/SUPPL_FILE/AO0C03663_SI_001.PDF.
[5] R. Malik, N. Joshi, V.K. Tomer, Advances in the designs and mechanisms of MoO3 nanostructures for gas sensors: a holistic review, Mater Adv 2 (2021) 4190–4227, https://doi.org/10.1039/D1MA00374G.
[6] C. Zhang, J. Sun, Y. Lu, J. Liu, Nanocrack-based strain sensors, J Mater Chem C Mater 9 (2021) 754–772, https://doi.org/10.1039/D0TC04346J.
[7] C. Anichini, W. Czepa, D. Pakulski, A. Aliprandi, A. Ciesielski, P. Samorì, Chemical sensing with 2D materials, Chem. Soc. Rev. 47 (2018) 4860–4908, https://doi.org/10.1039/C8CS00417J.

[8] M. Subash, M. Chandrasekar, S. Panimalar, C. Inmozhi, K. Parasuraman, R. Uthrakumar, K. Kaviyarasu, Pseudo-first kinetics model of copper doping on the structural, magnetic, and photocatalytic activity of magnesium oxide nanoparticles for energy application, Biomass Convers Biorefin 13 (2023) 3427–3437, https://doi.org/10.1007/S13399-022-02993-1.

[9] A. Mirzaei, J.H. Kim, H.W. Kim, S.S. Kim, Resistive-based gas sensors for detection of benzene, toluene and xylene (BTX) gases: a review, J Mater Chem C Mater 6 (2018) 4342–4370, https://doi.org/10.1039/C8TC00245B.

[10] H. Tang, Y. Li, R. Sokolovskij, L. Sacco, H. Zheng, H. Ye, H. Yu, X. Fan, H. Tian, T. L. Ren, G. Zhang, Ultra-high sensitive NO2 gas sensor based on tunable polarity transport in CVD-WS2/IGZO p-N heterojunction, ACS Appl. Mater. Interfaces 11 (2019) 40850–40859, https://doi.org/10.1021/ACSAMI.9B13773/SUPPL_FILE/AM9B13773_SI_001.PDF.

[11] J. Xie, L. Zhang, B. Liu, P. Bai, C. Wang, J. Xu, H. Wang, Highly selective gas sensor based on hydrophobic silica decorated with trimethoxyoctadecylsilane, ACS Appl. Mater. Interfaces 13 (2021) 1956–1966, https://doi.org/10.1021/ACSAMI.0C18582/SUPPL_FILE/AM0C18582_SI_001.PDF.

[12] M. Thepnurat, T. Chairuangsri, N. Hongsith, P. Ruankham, S. Choopun, Realization of interlinked ZnO tetrapod networks for UV sensor and room-temperature gas sensor, ACS Appl. Mater. Interfaces 7 (2015) 24177–27184, https://doi.org/10.1021/ACSAMI.5B07491/ASSET/IMAGES/MEDIUM/AM-2015-074917_0011.GIF.

[13] D. Lee, M.J. Yun, K.H. Kim, S. Kim, H.D. Kim, Advanced recovery and high-sensitive properties of memristor-based gas sensor devices operated at room temperature, ACS Sens. 6 (2021) 4217–4224, https://doi.org/10.1021/ACSSENSORS.1C01840/SUPPL_FILE/SE1C01840_SI_001.PDF.

[14] D. Klemm, B. Heublein, H.P. Fink, A. Bohn, Cellulose: fascinating biopolymer and sustainable raw material, Angewandte Chemie - International Edition 44 (2005) 3358–3393, https://doi.org/10.1002/anie.200460587.

[15] Paper Diagnostics Market Size & Analysis, Industry report, 2018-2025, n.d. https://www.grandviewresearch.com/industry-analysis/paper-diagnostics-market. (Accessed 18 November 2020).

[16] H. Golmohammadi, E. Morales-Narváez, T. Naghdi, A. Merkoçi, Nanocellulose in sensing and biosensing, Chem. Mater. 29 (2017) 5426–5446, https://doi.org/10.1021/acs.chemmater.7b01170.

[17] H. Dong, J.L. Terrell, J.P. Jahnke, T.N.K. Zu, M.M. Hurley, D.N. Stratis-Cullum, Biofunctionalized cellulose nanofibrils capable of capture and antiadhesion of fimbriated Escherichia coli, ACS Appl. Bio Mater. 2 (2019) 2937–2945, https://doi.org/10.1021/acsabm.9b00295.

[18] B. Thomas, M.C. Raj, B.K. Athira, H.M. Rubiyah, J. Joy, A. Moores, G.L. Drisko, C. Sanchez, Nanocellulose, a versatile green platform: from biosources to materials and their applications, Chem Rev 118 (2018) 11575–11625, https://doi.org/10.1021/acs.chemrev.7b00627.

[19] L.R. Lynd, P.J. Weimer, W.H. Van Zyl, I.S. Pretorius, Microbial cellulose utilization: fundamentals and biotechnology, MICROBIOLOGY AND MOLECULAR BIOLOGY REVIEWS 66 (2002) 506–577, https://doi.org/10.1128/MMBR.66.3.506-577.2002.

[20] D. Klemm, F. Kramer, S. Moritz, T. Lindström, M. Ankerfors, D. Gray, A. Dorris, Nanocelluloses: a new family of nature-based materials, Angewandte Chemie - International Edition 50 (2011) 5438–5466, https://doi.org/10.1002/anie.201001273.

[21] R.J. Moon, A. Martini, J. Nairn, J. Simonsen, J. Youngblood, Cellulose nanomaterials review: structure, properties and nanocomposites, Chem. Soc. Rev. 40 (2011) 3941–3994, https://doi.org/10.1039/c0cs00108b.

[22] M. Yan, W. Qu, Q. Su, S. Chen, Y. Xing, Y. Huang, N. Chen, Y. Li, L. Li, F. Wu, R. Chen, Biodegradable bacterial cellulose-supported quasi-solid electrolyte for lithium batteries, ACS Appl. Mater. Interfaces 12 (2020) 13950–13958, https://doi.org/10.1021/acsami.0c00621.

[23] H. Wei, K. Rodriguez, S. Renneckar, P.J. Vikesland, Environmental science and engineering applications of nanocellulose-based nanocomposites, Environ. Sci.: Nano 1 (2014) 302–316, https://doi.org/10.1039/c4en00059e.

[24] E. Morales-Narváez, H. Golmohammadi, T. Naghdi, H. Yousefi, U. Kostiv, D. Horák, N. Pourreza, A. Merkoçi, Nanopaper as an optical sensing platform, ACS Nano 9 (2015) 7296–7305, https://doi.org/10.1021/acsnano.5b03097.

[25] R. Rahighi, M. Panahi, O. Akhavan, M. Mansoorianfar, Pressure-engineered electrophoretic deposition for gentamicin loading within osteoblast-specific cellulose nanofiber scaffolds, Mater. Chem. Phys. 272 (2021) 125018, https://doi.org/10.1016/J.MATCHEMPHYS.2021.125018.

[26] A. Al-Nayili, S.A. Haimd, Design of a new ZnCo2O4 nanoparticles/nitrogen-rich g-C3N4 sheet with improved photocatalytic activity under visible light, J Clust Sci 35 (2024) 341–358, https://doi.org/10.1007/S10876-023-02487-8.

[27] A. Sabarinathan, M.C.-I.C., undefined, An Effective Photocatalytic Degradation of Methylene Blue with ZnO/SnO2–CeO2/CuO Quaternary Nanocomposite Driven by Visible Light Irradiation, Elsevier, 2023 n.d. https://www.sciencedirect.com/science/article/pii/S1387700323007761?casa_token=oBu_HyHU7zIAAAAA:9thdfI_J6PFt4aPIq_DyCZWGIt6I3AgLIyew83osgFJRmN3c-Q9wqbZkIlqqjtgaQdMkv9aDQ. (Accessed 14 April 2024).

[28] K. Kaviyarasu, M.S. Elshikh, Saeedah, M. Almutairi, · R. Uthrakumar, A. Muthukumaran, Reactive oxygen species (ROS) are generated as organic contaminants are broken down: SnO2-doped graphene oxide nanocomposites are investigated under, SpringerK kaviyarasu, in: M.S. Elshikh, S.M. Almutairi, R. Uthrakumar, A. Muthukumaran (Eds.), BioNanoScience, 2023•Springer 13 (2023) 920–928, https://doi.org/10.1007/s12668-023-01111-3.

[29] S. Panimalar, M. Subash, M.C.- Chemosphere, undefined, Reproducibility and Long-Term Stability of Sn Doped MnO2 Nanostructures: Practical Photocatalytic Systems and Wastewater Treatment Applications, ElsevierS Panimalar, M Subash, M Chandrasekar, R Uthrakumar, C Inmozhi, WA Al-OnaziChemosphere, 2022•Elsevier, 2022 n.d. https://www.sciencedirect.com/science/article/pii/S0045653522001394?casa_token=lB6VLJZ3HxsAAAAA:CG6fvoRVskU6_TslfBQaQUamwOUgTW0eVxlgezbI3N5wmhYQXvyWlucMGMvTMbh4vHTU_TJPUw. (Accessed 14 April 2024).

[30] G. Siqueira, J. Bras, A. Dufresne, Cellulosic bionanocomposites: a review of preparation, properties and applications, Polymers 2 (2010) 728–765, https://doi.org/10.3390/polym2040728.

[31] J. Bras, M.L. Hassan, C. Bruzesse, E.A. Hassan, N.A. El-Wakil, A. Dufresne, Mechanical, barrier, and biodegradability properties of bagasse cellulose whiskers reinforced natural rubber nanocomposites, Ind. Crops Prod. 32 (2010) 627–633, https://doi.org/10.1016/j.indcrop.2010.07.018.

[32] H. Wei, K. Rodriguez, S. Renneckar, P.J. Vikesland, Environmental science and engineering applications of nanocellulose-based nanocomposites, Environ. Sci.: Nano 1 (2014) 302–316, https://doi.org/10.1039/c4en00059e.

[33] Y.H. Kim, D.G. Moon, J.I. Han, Organic TFT array on a paper substrate, IEEE Electron. Device Lett. 25 (2004) 702–704, https://doi.org/10.1109/LED.2004.836502.

[34] E. Rodríguez-Sevilla, G.V. Vázquez, E. Morales-Narváez, Simple, flexible, and ultrastable surface enhanced Raman scattering substrate based on plasmonic nanopaper decorated with graphene oxide, Adv. Opt. Mater. 6 (2018) 1800548, https://doi.org/10.1002/adom.201800548.

[35] W. Kang, M.-F. Lin, J. Chen, P.S. Lee, Highly transparent conducting nanopaper for solid state foldable electrochromic devices, Small 12 (2016) 6370–6377, https://doi.org/10.1002/smll.201600979.

[36] D.H. Lien, Z.K. Kao, T.H. Huang, Y.C. Liao, S.C. Lee, J.H. He, All-printed paper memory, ACS Nano 8 (2014) 7613–7619, https://doi.org/10.1021/nn501231z.

[37] L. Yang, S. Cheng, Y. Ding, X. Zhu, Z.L. Wang, M. Liu, Hierarchical network architectures of carbon fiber paper supported cobalt oxide nanonet for high-capacity pseudocapacitors, Nano Lett. 12 (2012) 321–325, https://doi.org/10.1021/nl203600x.

[38] A.C. Siegel, S.T. Phillips, M.D. Dickey, N. Lu, Z. Suo, G.M. Whitesides, Foldable printed circuit boards on paper substrates, Adv. Funct. Mater. 20 (2010) 28–35, https://doi.org/10.1002/adfm.200901363.

[39] R. Martins, I. Ferreira, E. Fortunato, Electronics with and on paper, Phys. Status Solidi Rapid Res. Lett. 5 (2011) 332–335, https://doi.org/10.1002/pssr.201105247.

[40] J. Xue, F. Song, X.W. Yin, X.L. Wang, Y.Z. Wang, Let it shine: a transparent and photoluminescent foldable nanocellulose/quantum dot paper, ACS Appl. Mater. Interfaces 7 (2015) 10076–10079, https://doi.org/10.1021/acsami.5b02011.

[41] M. Nogi, N. Komoda, K. Otsuka, K. Suganuma, Foldable nanopaper antennas for origami electronics, Nanoscale 5 (2013) 4395–4399, https://doi.org/10.1039/c3nr00231d.

[42] Q. Cheng, Z. Song, T. Ma, B.B. Smith, R. Tang, H. Yu, H. Jiang, C.K. Chan, Folding paper-based lithium-ion batteries for higher areal energy densities, Nano Lett. 13 (2013) 4969–4974, https://doi.org/10.1021/nl4030374.

[43] M.T. Maurano, E. Haugen, R. Sandstrom, J. Vierstra, A. Shafer, R. Kaul, J. A. Stamatoyannopoulos, Large-scale identification of sequence variants influencing human transcription factor occupancy in vivo, Nat. Genet. (2015), https://doi.org/10.1038/ng.3432.

[44] Y. Li, H. Zhu, H. Gu, H. Dai, Z. Fang, N.J. Weadock, Z. Guo, L. Hu, Strong transparent magnetic nanopaper prepared by immobilization of Fe 3O4 nanoparticles in a nanofibrillated cellulose network, J Mater Chem A Mater 1 (2013) 15278–15283, https://doi.org/10.1039/c3ta12591b.

[45] A. Brakat, H. Zhu, Nanocellulose-graphene hybrids: advanced functional materials as multifunctional sensing platform, Nano-Micro Lett. 13 (2021) 1–37, https://doi.org/10.1007/s40820-021-00627-1.

[46] A. Nasri, M. Pétrissans, V. Fierro, A. Celzard, Gas sensing based on organic composite materials: review of sensor types, progresses and challenges, Mater. Sci. Semicond. Process. 128 (2021) 105744, https://doi.org/10.1016/j.mssp.2021.105744.

[47] C.N. Wu, S.C. Fuh, S.P. Lin, Y.Y. Lin, H.Y. Chen, J.M. Liu, K.C. Cheng, TEMPO-oxidized bacterial cellulose pellicle with silver nanoparticles for wound dressing, Biomacromolecules 19 (2018) 544–554, https://doi.org/10.1021/ACS.BIOMAC.7B01660/ASSET/IMAGES/MEDIUM/BM-2017-01660P_0012.GIF.

[48] M. Chen, H. Kang, Y. Gong, J. Guo, H. Zhang, R. Liu, Bacterial cellulose supported gold nanoparticles with excellent catalytic properties, ACS Appl. Mater. Interfaces 7 (2015) 21717–21726, https://doi.org/10.1021/ACSAMI.5B07150/SUPPL_FILE/AM5B07150_SI_001.PDF.

[49] H. Gholami Derami, P. Gupta, R. Gupta, P. Rathi, J.J. Morrissey, S. Singamaneni, Palladium nanoparticle-decorated mesoporous polydopamine/bacterial nanocellulose as a catalytically active universal dye removal ultrafiltration membrane, ACS Appl. Nano Mater. 3 (2020) 5437–5448, https://doi.org/10.1021/ACSANM.0C00787/SUPPL_FILE/AN0C00787_SI_001.PDF.

[50] C. Mira-Cuenca, T. Meslier, S. Roig-Sanchez, A. Laromaine, A. Roig, Patterning bacterial cellulose films with iron oxide nanoparticles and magnetic resonance imaging monitoring, ACS Appl. Polym. Mater. 3 (2021) 4959–4965, https://doi.org/10.1021/ACSAPM.1C00723/ASSET/IMAGES/LARGE/AP1C00723_0006.JPEG.

[51] H. Kim, G.H. Kwon, S.O. Han, A. Robertson, Platinum encapsulated within a bacterial nanocellulosic-graphene nanosandwich as a durable thin-film fuel cell catalyst, ACS Appl. Energy Mater. 4 (2021) 1286–1293, https://doi.org/10.1021/ACSAEM.0C02533/SUPPL_FILE/AE0C02533_SI_001.PDF.

[52] E. Morales-Narváez, H. Golmohammadi, T. Naghdi, H. Yousefi, U. Kostiv, D. Horák, N. Pourreza, A. Merkoçi, Nanopaper as an optical sensing platform, ACS

Nano 9 (2015) 7296–7305, https://doi.org/10.1021/ACSNANO.5B03097/SUPPL_FILE/NN5B03097_SI_001.PDF.
[53] M. Shah, J. Khan, M. Sajjad, M. Kazi, K.T.-J. of P. and, undefined, Methylene Blue-Based Multifunctional Sensor for Sensitive Detection of Organic Solvents and Gases, Elsevier, 2024 n.d. https://www.sciencedirect.com/science/article/pii/S0022369724000805?casa_token=X2Jq3H2s_VcAAAAA:Gm8EM0ppQVrcu3UlOxoBibasnjj2czfA0tIJSsOpTsxnGF7KIllw3EBqPTnUzMZd4OPSBmfAUw. (Accessed 13 April 2024).
[54] D. Janwery, F. Hussain Memon, A. Ali Memon, M. Iqbal, F. Nisa Memon, W. Ali, K.-H. Choi, K. Hussain Thebo, Lamellar graphene oxide-based composite membranes for efficient separation of heavy metal ions and desalination of water, ACS Publications, in: D. Janwery, F.H. Memon, A.A. Memon, M. Iqbal, F. N. Memon, W. Ali, K.H. Choi, K.H. Thebo (Eds.), ACS Omega, 2023•ACS Publications, 2023, pp. 7648–7656, https://doi.org/10.1021/acsomega.2c07243, 8.
[55] F.A. Janjhi, D. Janwery, I. Chandio, S. Ullah, F. Rehman, A.A. Memon, J. Hakami, F. Khan, G. Boczkaj, K.H. Thebo, Recent advances in graphene oxide-based membranes for heavy metal ions separation, ChemBioEng Rev. 9 (2022) 574–590, https://doi.org/10.1002/CBEN.202200015.
[56] M.U.N. Khilji, N.A. Nahyoon, M. Mehdi, K.H. Thebo, N. Mahar, A.A. Memon, N. Memon, N. Hussain, Synthesis of novel visible light driven MgO@GO nanocomposite photocatalyst for degradation of Rhodamine 6G, Opt. Mater. 135 (2023), https://doi.org/10.1016/J.OPTMAT.2022.113260.
[57] I. Mahar, F. Hussain Memon, J.-W. Lee, K.H. Kim, R. Ahmed, F. Soomro, F. Rehman, A.A. Memon, K. Hussain Thebo, K.H. Choi, O. Arzhakova, P.S. Goh, A. A.M. Pk, Two-dimensional transition metal carbides and nitrides (MXenes) for water purification and antibacterial applications, Mdpi.Com, in: I. Mahar, F. H. Memon, J.W. Lee, K.H. Kim, R. Ahmed, F. Soomro, F. Rehman, A.A. Memon (Eds.), Membranes, 2021•mdpi.Com 11, 2021, https://doi.org/10.3390/membranes11110869.
[58] M.K. Shahzad, F.H. Memon, F. Soomro, M. Iqbal, A. Ibrar, A.A. Memon, J.H. Lim, K.H. Choi, K.H. Thebo, MoS2-based lamellar membranes for mass transport applications: challenges and opportunities, J. Environ. Chem. Eng. 11 (2023), https://doi.org/10.1016/J.JECE.2023.109329.
[59] F. Rehman, F. Hussain Memon, S. Ullah, M.A. Jafar Mazumder, A. Al-Ahmed, F. Khan, K. Hussain Thebo, Recent development in laminar transition metal dichalcogenides-based membranes towards water desalination: a review, Chem. Rec. 22 (2022), https://doi.org/10.1002/TCR.202200107.
[60] I. Mahar, F.K. Mahar, N. Mahar, A.A. Memon, A.A.A. Pirzado, Z. Khatri, K. H. Thebo, A. Ali, Fabrication and characterization of MXene/carbon composite-based nanofibers (MXene/CNFs) membrane: an efficient adsorbent material for removal of Pb+2 and As+3 ions from water, Chem. Eng. Res. Des. 191 (2023) 462–471, https://doi.org/10.1016/J.CHERD.2023.02.005.
[61] A. Ali, F. Rehman, M. Ali Khan, F. Hussain Memon, F. Soomro, M. Iqbal, J. Yang, K. Hussain Thebo, Functionalized graphene oxide-based lamellar membranes with tunable nanochannels for ionic and molecular separation, ACS Publications, in: A. Ali, F. Rehman, M. Ali Khan, F.H. Memon, F. Soomro, M. Iqbal, J. Yang (Eds.), KH TheboACS Omega, 2022•ACS Publications 7, 2022, pp. 32410–32417, https://doi.org/10.1021/acsomega.2c03907.
[62] F. Rehman, F.H. Memon, Z. Bhatti, M. Iqbal, F. Soomro, A. Ali, K.H. Thebo, Graphene-based composite membranes for isotope separation: challenges and opportunities, Rev. Inorg. Chem. 42 (2022) 327–336, https://doi.org/10.1515/REVIC-2021-0035/HTML.
[63] A.H. Jatoi, K.H. Kim, B. Muhammad, A. Khan, F. Hussain, D. Janwery, S. N. Phulpoto, A. Samantasinghar, K.H. Choi, K.H. Thebo, Functionalized graphene oxide-based lamellar membranes for organic solvent nanofiltration applications, Pubs.Rsc.Org, in: A.H. Jatoi, K.H. Kim, M.A. Khan, F.H. Memon, M. Iqbal, D. Janwery, S.N. Phulpoto (Eds.), RSC Advances, 2023•pubs.Rsc.Org 13, 2023, pp. 12695–12702, https://doi.org/10.1039/d3ra00223c.
[64] F. Soomro, A. Ali, S. Ullah, M. Iqbal, T. Alshahrani, F. Khan, J. Yang, K. Hussain Thebo, Highly efficient arginine intercalated graphene oxide composite membranes for water desa, in: F. Soomro, A. Ali, S. Ullah, M. Iqbal, T. Alshahrani, F. Khan, J. Yang, K.H. Thebo (Eds.), Langmuir, 2023•ACS Publications 39, 2023, pp. 18447–18457, https://doi.org/10.1021/acs.langmuir.3c02699.
[65] A. Hyder, A. Ali, A. Khalid, A. Nadeem, M. Ali Khan, A. Wahab Memon, A. Ali Memon, D. Janwery, M. Mehdi, A. Solangi, J. Yang, K. Hussain Thebo, Supramolecular structural-based graphene oxide lamellar membrane for removing environmental pollutants from wastewater, in: A. Hyder, A. Ali, A. Khalid, A. Nadeem, M.A. Khan, A.W. Memon, A.A. Memon, D. Janwery, M. Mehdi (Eds.), Industrial & Engineering Chemistry Research, 2023•ACS Publications 62, 2023, pp. 21335–21346, https://doi.org/10.1021/acs.iecr.3c03260.
[66] M.U.N. Khilji, A.A. Otho, R. Memon, A. Khalid, M. Kazi, A. Hyder, D. Janwery, N. A. Nahyoon, A.A. Memon, N. Memon, K.H. Thebo, Facile fabrication of a free-standing magnesium oxide-graphene oxide functionalized membrane: a robust and efficient material for the removal of pollutants from aqueous matrices, Anal. Lett. (2023), https://doi.org/10.1080/00032719.2023.2284841.
[67] A.H. Jatoi, A. Ali, A. Nadeem, S.N. Phulpoto, M. Iqbal, F. Ayaz, A. Memon, J. Yang, K.H. Thebo, High-performance asparagine-modified graphene oxide membranes for organic dyes and heavy metal ion separation, Pubs.Rsc.Org, in: A. H. Jatoi, A. Ali, A. Nadeem, S.N. Phulpoto, M. Iqbal, A.A. Memon, J. Yang (Eds.), KH TheboNew Journal of Chemistry, 2024•pubs.Rsc.Org 48, 2024, p. 1715, https://doi.org/10.1039/d3nj04552h.
[68] A. Hyder, M. Thebo, D. Janwery, J. Ahmed Buledi, I. Chandio, A. Khalid, B.S. Al-Anzi, H.A. Almukhlifi, K. Hussain Thebo, F.N. Memon, A. Ali Memon, A. Rehana Solangi, S. Memon, Arene functionalized self-assembled graphene oxide composite material for effective removal of 2, 4, 6-tri, Cell.Com, in: A. Hyder, M. Thebo, D. Janwery, J.A. Buledi, I. Chandio, A. Khalid, B.S. Al-Anzi, H. A. Almukhlifi (Eds.), Heliyon, 2023•cell.Com, 2023, https://doi.org/10.1016/j.heliyon.2023.e19622.
[69] Q. Zhang, X. Qian, K. Thebo, H. Cheng, W.R.-S. bulletin, undefined, Controlling Reduction Degree of Graphene Oxide Membranes for Improved Water Permeance, Elsevier, 2018 n.d. https://www.sciencedirect.com/science/article/pii/S2095927318302366?casa_token=XObDtoAf154AAAAA:tZh3GM80WlGkG5ndsBizqmfqXEG_kzUBIBCj2JVeAECVAcFiZ_tLs4oaTp2yXWvucWm-3m1IFQ. April 13, 2024
[70] J. Feng, B. Ye, L. Zuo, R. Qi, Q. Wang, H.J.-J. of M., undefined, Effects of Zr, Ti and Sc additions on the microstructure and mechanical properties of Al-0.4 Cu-0.14 Si-0.05 Mg-0.2 Fe alloys, Elsevier, in: J. Feng, B. Ye, L. Zuo, R. Qi, Q. Wang, H. Jiang, R. Huang, W. Ding, J. Yao, C. Wang (Eds.), Journal of Materials Science & Technology, 2018, Elsevier (n.d.), 2018. https://www.sciencedirect.com/science/article/pii/S1005030218301269?casa_token=vh-CguzJDFwAAAAA:_m6TEjWeJVpojfJX8A_8SLA83n16I_SuvcMaEcGNdZfq08MnvU_mvA-4EPSmqPvzIgzmnM4Gew. (Accessed 13 April 2024).
[71] S. Sharif, K. Ahmad, F. Rehman, Z.B.-J. of E., undefined, Two-dimensional graphene oxide based membranes for ionic and molecular separation: current status and challenges, Elsevier, in: S. Sharif, K.S. Ahmad, F. Rehman, Z. Bhatti (Eds.), KH TheboJournal of Environmental Chemical Engineering, 2021, Elsevier, 2021 n.d. https://www.sciencedirect.com/science/article/pii/S2213343721005820?casa_token=TW-mEegiDnMAAAAA:nKALlVlTgW_C50Xu6WjIBHH5wZcct-TKcSCxkrc8bt1bGBs_YwYyRSoXcZ5OEQKfRtCWmjEm1w. (Accessed 13 April 2024).
[72] C. Anjali, V. Nidhisha, T. Amrutha, R.G.-R. in, undefined, Graphene oxide boosted high surface area CeO2 for humidity sensing, Elsevier, in: C. Anjali, V. Nidhisha, T.P. Amrutha, R. Gopal, B. Chethan, M.S. Thayyil, P. Periyat (Eds.), RN KizhakayilResults in Engineering, 2024•Elsevier (n.d.), 2024. https://www.sciencedirect.com/science/article/pii/S2590123024000057. (Accessed 18 April 2024).
[73] V.P. Haritha, V. Haridas, K.V. Snisha, P.V. Suraja, N.K. Renuka, N.N. Binitha, β-Co(OH)2–Co3O4/Graphene Oxide 3D-Nanoarchitecture modified electrode for electrochemical sensing and energy storage applications, Results in Engineering 19 (2023) 101391, https://doi.org/10.1016/J.RINENG.2023.101391.
[74] M.K. Shabbir, W. Ali, U. Khanum, K.H. Memon, J. Akhtar, M. Iqbal, F. Bhutta, J. M. Ashfaq, K.H. Choi, K.H. Thebo, Facile synthesis of SnO2/graphene and Bi–SnO2/graphene-based nanocomposites as electrode materials for energy storage devices, Results in Engineering 20 (2023) 101520, https://doi.org/10.1016/J.RINENG.2023.101520.
[75] C. Vijina, S.D.-R. in Engineering, Platinum nanoparticle-decorated reduced graphene oxide nanosheets: a recyclable and highly efficient catalyst towards the reduction of para-nitrophenol and, ElsevierC Vijina, SP DamodaranResults in Engineering, Elsevier 20 (2023) 101444. https://www.sciencedirect.com/science/article/pii/S2590123023005716 (Accessed 18 April 2024).
[76] N.A. Elessawy, M. Abdel Rafea, N. Roushdy, M.E. Youssef, M.H. Gouda, Development and evaluation of cost-effective and green Bi-functional nickel oxide decorated graphene electrocatalysts for alkaline fuel cells, Results in Engineering 17 (2023) 100871, https://doi.org/10.1016/J.RINENG.2022.100871.
[77] M. Aghaee Malayeri, H. Koohestani, M. Tajally, Improving the properties of nickel/graphene oxide coated copper plate by changing the electroplating process conditions, Results in Engineering 18 (2023) 101167, https://doi.org/10.1016/J.RINENG.2023.101167.
[78] M. Alishiri, S.A. Abdollahi, A.N. Neysari, S.F. Ranjbar, N. Abdoli, M. Afsharjahanshahi, Removal of ciprofloxacin and cephalexin antibiotics in water environment by magnetic graphene oxide nanocomposites; optimization using response surface methodology, Results in Engineering 20 (2023) 101507, https://doi.org/10.1016/J.RINENG.2023.101507.
[79] B. M, P. Periyat, Graphene and its derivatives for air purification: a mini review, Results in Engineering 21 (2024) 101809, https://doi.org/10.1016/J.RINENG.2024.101809.
[80] H. Abdali, B. Heli, A.A.- Sensors, undefined, Cellulose nanopaper cross-linked amino graphene/polyaniline sensors to detect CO2 gas at room temperature, Mdpi.ComH Abdali, B Heli, A AjjiSensors, 2019•mdpi.Com (2019), https://doi.org/10.3390/s19235215 (n.d.).
[81] B. Xu, J. Huang, L. Ding, H. Zhang, H. Zhang, A sensitive ammonia sensor using long period fiber grating coated with graphene oxide/cellulose acetate, IEEE Sens J 21 (2021) 16691–16700, https://doi.org/10.1109/JSEN.2021.3081745.
[82] S. Dacrory, A. Saeed, R.A.-E.P. Letters, undefined, A novel ammonia sensor based on cellulose/graphene oxide functionalized with ethylenediamine, Real.Mtak.Hu (n.d.) (2022), https://doi.org/10.3144/expresspolymlett.2022.58.
[83] A. Jain, S. Panda, Y. Zhao, H.-Y. Li, J. Liu, Q. Zhang, C. An, S. Fan, S. Shi, R. Zhang, J. Zhang, Q. Li, D. Zhang, X. Hu, J. Liu, Flexible gas sensor based on graphene/ethyl cellulose nanocomposite with ultra-low strain response for volatile organic compounds rapid detection, Iopscience.Iop.Org, in: Q. Zhang, C. An, S. Fan, S. Shi, R. Zhang, J. Zhang, Q. Li, D. Zhang, X. Hu, J. Liu (Eds.), Nanotechnology, 2018•iopscience.Iop.Org 29, 2018, https://doi.org/10.1088/1361-6528/aabf2f.
[84] S. Duan, K. Yang, Z. Wang, M. Chen, L. Zhang, H. Zhang, C. Li, Fabrication of highly stretchable conductors based on 3D printed porous poly(dimethylsiloxane) and conductive carbon nanotubes/graphene network, ACS Appl. Mater. Interfaces 8 (2016) 2187–2192, https://doi.org/10.1021/ACSAMI.5B10791/SUPPL_FILE/AM5B10791_SI_001.PDF.
[85] J. Prakash, U. Prasad, R. Alexander, J. Bahadur, K. Dasgupta, A.N.M. Kannan, Photoelectrochemical solar water splitting: the role of the carbon nanomaterials

in bismuth vanadate composite photoanodes toward efficient charge separation and transport, Langmuir 35 (2019) 14492–14504, https://doi.org/10.1021/ACS.LANGMUIR.9B02782/SUPPL_FILE/LA9B02782_SI_001.PDF.
[86] W. Shao, S. Wang, H. Liu, J. Wu, R. Zhang, H. Min, M. Huang, Preparation of bacterial cellulose/graphene nanosheets composite films with enhanced mechanical performances, Carbohydr. Polym. (2016), https://doi.org/10.1016/j.carbpol.2015.11.033.
[87] D. Düzenli, A comparative density functional study of hydrogen peroxide adsorption and activation on the graphene surface doped with N, B, S, Pd, Pt, Au, Ag, and Cu atoms, J. Phys. Chem. C 120 (2016) 20149–20157, https://doi.org/10.1021/ACS.JPCC.6B06131/SUPPL_FILE/JP6B06131_SI_001.PDF.
[88] J.H. Choi, J. Lee, M. Byeon, T.E. Hong, H. Park, C.Y. Lee, Graphene-based gas sensors with high sensitivity and minimal sensor-to-sensor variation, ACS Appl. Nano Mater. 3 (2020) 2257–2265, https://doi.org/10.1021/ACSANM.9B02378/SUPPL_FILE/AN9B02378_SI_001.PDF.
[89] S. Zhu, Q. Meng, L. Wang, J. Zhang, Y. Song, H. Jin, K. Zhang, H. Sun, H. Wang, B. Yang, Highly photoluminescent carbon dots for multicolor patterning, sensors, and bioimaging, Angewandte Chemie - International Edition (2013), https://doi.org/10.1002/anie.201300519.
[90] S.Y. Lim, W. Shen, Z. Gao, Carbon quantum dots and their applications, Chem. Soc. Rev. (2015), https://doi.org/10.1039/c4cs00269e.
[91] O.S. Wolfbeis, An overview of nanoparticles commonly used in fluorescent bioimaging, Chem. Soc. Rev. (2015), https://doi.org/10.1039/c4cs00392f.
[92] A. Esfandiar, N. Kybert, E. Dattoli, G.H.H.-A.P., undefined, DNA-decorated graphene nanomesh for detection of chemical vapors, Pubs.Aip.Org 103 (2013) 183110. https://pubs.aip.org/aip/apl/article/103/18/183110/129939 (Accessed 14 April 2024).
[93] R. Rahighi, O. Akhavan, A.S. Zeraati, S.M. Sattari-Esfahlan, All-carbon negative differential resistance nanodevice using a single flake of nanoporous graphene, ACS Appl. Electron. Mater. 3 (2021) 3418–3427, https://doi.org/10.1021/ACSAELM.1C00396/ASSET/IMAGES/LARGE/EL1C00396_0007.JPEG.
[94] D.C. Marcano, D.V. Kosynkin, J.M. Berlin, A. Sinitskii, Z. Sun, A. Slesarev, L. B. Alemany, W. Lu, J.M. Tour, Improved synthesis of graphene oxide, ACS Nano (2010), https://doi.org/10.1021/nn1006368.
[95] S. Abdolhosseinzadeh, H. Asgharzadeh, H.S. Kim, Fast and fully-scalable synthesis of reduced graphene oxide, Sci. Rep. 5 (2015), https://doi.org/10.1038/srep10160.
[96] L. Baptista-Pires, C.C. Mayorga-Martínez, M. Medina-Sánchez, H. Montón, A. Merkoçi, Water activated graphene oxide transfer using wax printed membranes for fast patterning of a touch sensitive device, ACS Nano (2016), https://doi.org/10.1021/acsnano.5b05963.
[97] K. Kaviyarasu, M.S. Elshikh, Saeedah, M. Almutairi, R. Uthrakumar, A. Muthukumaran, Reactive oxygen species (ROS) are generated as organic contaminants are broken down: SnO2-doped graphene oxide nanocomposites are investigated under, SpringerK kaviyarasu, in: M.S. Elshikh, S.M. Almutairi, R. Uthrakumar, A. Muthukumaran (Eds.), BioNanoScience, Springer, 2023, pp. 920–928, https://doi.org/10.1007/s12668-023-01111-3, 13 (2023).
[98] E. Zor, S. Alpaydin, A. Arici, M.E. Saglam, H. Bingol, Photoluminescent nanopaper-based microcuvette for iodide detection in seawater, Sens Actuators B Chem (2018), https://doi.org/10.1016/j.snb.2017.07.208.
[99] A.F. Leitão, J.P. Silva, F. Dourado, M. Gama, Production and characterization of a new bacterial cellulose/poly(Vinyl Alcohol) nanocomposite, Materials 6 (2013) 1956–1966, https://doi.org/10.3390/ma6051956.
[100] Q. Fang, X. Zhou, W. Deng, Z. Zheng, Z. Liu, Freestanding bacterial cellulose-graphene oxide composite membranes with high mechanical strength for selective ion permeation, Sci. Rep. 6 (2016), https://doi.org/10.1038/srep33185.
[101] R.L. Oliveira, J.G. Vieira, H.S. Barud, R.M.N. Assunção, G.R. Filho, S.J.L. Ribeiro, Y. Messadeqq, Synthesis and characterization of methylcellulose produced from bacterial cellulose under heterogeneous condition, J. Braz. Chem. Soc. 26 (2015) 1861–1870, https://doi.org/10.5935/0103-5053.20150163.
[102] C. Katepetch, R. Rujiravanit, H. Tamura, Formation of nanocrystalline ZnO particles into bacterial cellulose pellicle by ultrasonic-assisted in situ synthesis, Cellulose 20 (2013) 1275–1292, https://doi.org/10.1007/s10570-013-9892-8.
[103] T. Zhang, G.Y. Zhu, C.H. Yu, Y. Xie, M.Y. Xia, B.Y. Lu, X. Fei, Q. Peng, The UV absorption of graphene oxide is size-dependent: possible calibration pitfalls, Microchim. Acta 186 (2019) 1–7, https://doi.org/10.1007/s00604-019-3329-5.
[104] M. Shaban, M. Rabia, A.M. Abd El-Sayed, A. Ahmed, S. Sayed, A.M.A. El-Sayed, A. Ahmed, S. Sayed, Photocatalytic properties of PbS/graphene oxide/polyaniline electrode for hydrogen generation, Sci. Rep. 7 (2017) 14100, https://doi.org/10.1038/s41598-017-14582-8.
[105] S.E. Zaki, M.A. Basyooni, M. Shaban, M. Rabia, Y.R. Eker, G.F. Attia, M. Yilmaz, A.M. Ahmed, Role of oxygen vacancies in vanadium oxide and oxygen functional groups in graphene oxide for room temperature CO2 gas sensors, Sens Actuators A Phys 294 (2019) 17–24, https://doi.org/10.1016/j.sna.2019.04.037.
[106] M. Shaban, S. Ali, M. Rabia, Design and application of nanoporous graphene oxide film for CO2, H2, and C2H2 gases sensing, J. Mater. Res. Technol. 8 (2019) 4510–4520, https://doi.org/10.1016/j.jmrt.2019.07.064.
[107] A.M. El Sayed, M. Shaban, Structural, optical and photocatalytic properties of Fe and (Co, Fe) co-doped copper oxide spin coated films, Spectrochim. Acta Mol. Biomol. Spectrosc. 149 (2015) 638–646, https://doi.org/10.1016/j.saa.2015.05.010.
[108] M.A. Basyooni, M. Shaban, A.M. El Sayed, Enhanced gas sensing properties of spin-coated Na-doped ZnO nanostructured films, Sci. Rep. 7 (2017), https://doi.org/10.1038/srep41716.
[109] I. Talat, A. Arshad, Q. Mansoor, Graphene nanoplatelets/Cr2O3 nanocomposites as novel nanoantibiotics: towards control of multiple drug resistant bacteria, Ceram. Int. 47 (2021) 889–898, https://doi.org/10.1016/J.CERAMINT.2020.08.201.
[110] H. Cao, X. Qiu, Y. Liang, M. Zhao, Q. Zhu, Sol-gel synthesis and photoluminescence of p-type semiconductor Cr2O3 nanowires, Appl. Phys. Lett. 88 (2006) 241112, https://doi.org/10.1063/1.2213204.
[111] S. Khamlich, O. Nemraoui, N. Mongwaketsi, R. McCrindle, N. Cingo, M. Maaza, Black Cr/α-Cr2O3 nanoparticles based solar absorbers, Physica B Condens Matter 407 (2012) 1509–1512, https://doi.org/10.1016/J.PHYSB.2011.09.073.
[112] J. Singh, V. Verma, R. Kumar, S. Sharma, R. Kumar, Effect of structural and thermal disorder on the optical band gap energy of Cr2O3 nanoparticles, Mater. Res. Express 6 (2019) 085039, https://doi.org/10.1088/2053-1591/AB195C.
[113] R. Kalidoss, S. Umapathy, R. Anandan, V. Ganesh, Y. Sivalingam, Comparative study on the preparation and gas sensing properties of reduced graphene oxide/SnO 2 binary nanocomposite for detection of acetone in exhaled breath, Anal. Chem. 91 (2019) 5116–5124, https://doi.org/10.1021/acs.analchem.8b05670.
[114] M.A. Basyooni, S.E. Zaki, S. Ertugrul, M. Yilmaz, Y.R. Eker, Fast response of CO2 room temperature gas sensor based on Mixed-Valence Phases in Molybdenum and Tungsten Oxide nanostructured thin films, Ceram. Int. 46 (2020) 9839–9853, https://doi.org/10.1016/j.ceramint.2019.12.259.
[115] M.M. Mohammadi, A. Kumar, J. Liu, Y. Liu, T. Thundat, M.T. Swihart, Hydrogen sensing at room temperature using flame-synthesized palladium-decorated crumpled reduced graphene oxide nanocomposites, ACS Publications, in: M. M. Mohammadi, A. Kumar, J. Liu, Y. Liu, T. Thundat, M.T. Swihart (Eds.), ACS Sensors, ACS Publications, 2020, pp. 2344–2350, https://doi.org/10.1021/acssensors.0c01040, 5 (2020).
[116] A. Esfandiar, A. Irajizad, O. Akhavan, S. Ghasemi, M.R. Gholami, Pd-WO3/reduced graphene oxide hierarchical nanostructures as efficient hydrogen gas sensors, Int. J. Hydrogen Energy 39 (2014) 8169–8179, https://doi.org/10.1016/J.IJHYDENE.2014.03.117.